of the crystal shape factor seems also to be appropriate for the analysis of the fine structure of the diffraction spots of multiply twinned particles. Calculations to explain the results of experimental investigations of multiply twinned gold particles (Hofmeister, 1984) are in preparation.

The authors are grateful to Professor A. Delong and Professor V. Schmidt for continuing interest and suggestions promoting this cooperative work. They are especially indebted to Dr R. Hillebrand for permission to use his overprinting subroutine as part of our computer programs. Thanks are also due to Mrs Kolaříková for her assistance in preparing the typescript.

References

COWLEY, J. M. (1982). *Diffraction Physics*, 2nd ed., pp. 112, 187-191, 201-218. Amsterdam: North-Holland.

COWLEY, J. M., GOODMAN, P. & REES, A. L. G. (1957). *Acta Cryst.* **10**, 19-25.

EWALD, P. P. (1940). *Proc. Phys. Soc. London*, **52**, 167-174.

HOFMEISTER, H. (1984). *Thin Solid Films*, **116**, 151-162.

HOFMEISTER, H., HAEFKE, H. & KROHN, M. (1982). *J. Cryst. Growth*, **58**, 507-516.

HOFMEISTER, H., NEUMANN, W. & KOMRSKA, J. (1986). Tenth Eur. Crystallogr. Meet., Wrocław, Poland. Abstracts, pp. 371-372.

HOSEMANN, R. & BAGCHI, S. N. (1962). *Direct Analysis of Diffraction by Matter*, pp. 96-109. Amsterdam: North-Holland.

JAMES, R. W. (1967). *The Optical Principles of the Diffraction of X-rays*, p. 55. London: Bell.

KAMBE, K. & MOLIÈRE, K. (1970). *Dynamical Theory of Electron Diffraction*. In *Advances in Structure Research by Diffraction Methods*, edited by R. BRILL & R. MASON, Vol. 3, pp. 53-100. Braunschweig: Vieweg.

KATO, N. (1952). *J. Phys. Soc. Jpn*, **7**, 397-406.

KOMRSKA, J. (1982). *J. Opt. Soc. Am.* **72**, 1382-1384; **73**, 864.

KOMRSKA, J. (1988). *Czech. J. Phys. B.* Submitted.

LAUE, M. VON (1936). *Ann. Phys. (Leipzig)* (5. *Folge*), **26**, 55-68.

LAUE, M. VON (1948). *Materiewellen und ihre Interferenzen*, 2nd ed., pp. 168-186. Leipzig: Akademische Verlagsgesellschaft Geest & Partig K-G.

LEHMPFUHL, G. & REISSLAND, A. (1968). *Z. Naturforsch. Teil A*, **23**, 544-549.

MOLIÈRE, K. & NIEHRS, H. (1954). *Z. Phys.* **137**, 445-462.

MOLIÈRE, K. & WAGENFELD, H. (1958). *Z. Kristallogr.* **110**, 175-196.

PATTERSON, A. L. (1939). *Phys. Rev.* **56**, 972-977.

RAETHER, H. (1957). *Elektroneninterferenzen*. In *Handbuch der Physik*, edited by S. FLÜGGE, Bd XXXII, *Strukturforschung*, pp. 443-551. Berlin: Springer-Verlag.

Acta Cryst. (1988). A**44**, 897-904

Stacking Disorder in a Stage-4 $FeCl_3$–Graphite Intercalation Compound

BY S. HASHIMOTO, K. FORSTER AND S. C. MOSS

Physics Department, University of Houston, Houston, TX 77004, *USA*

(*Received* 1 *December* 1987; *accepted* 10 *May* 1988)

Abstract

X-ray scattering measurements have been made *in situ* on highly oriented pyrolytic graphite intercalated with $FeCl_3$ to stage 4 in a sealed glass tube at 620 K. It has been found that the $FeCl_3$ is in a two-dimensional liquid state at this temperature and that the stacking of the sets of ordered graphite layers (*ABAB*) that bound the intercalant is nearly random. Through a novel modeling of L scans for $10.L$, $11.L$, $20.L$, $21.L$, $30.L$ and $22.L$, a good fit has been achieved by using 60% of a preferred (*A*-*A*) stacking of sets with a broad lateral distribution about the ordered position. The remaining 40% of the sets are stacked with complete translational randomness, without regard to the normal graphite crystallography. This sliding randomness remains compatible with Daumas-Herold domain formation.

I. Introduction

A variety of structural behavior appears in graphite intercalation compounds (GIC's) depending critically on the molecular nature of the species intercalated within the graphite host. With the acceptor compounds, there are often rather complex sequences of ordering reactions involving transitions from liquid to incommensurate solid to commensurate solid (Dresselhaus & Dresselhaus, 1981; Solin, 1982; Moret, 1986). In the case of $FeCl_3$, beginning with the early electron diffraction study by Cowley & Ibers (1956), there has been extensive structural characterization, mainly by Metz and co-workers (Hohlwein & Metz, 1974; Metz & Schulze, 1975; Metz & Hohlwein, 1975). A major feature of these photographic studies, common to all the GIC's, has been the occurrence of well defined stages in which, for

0108-7673/88/060897-08$03.00

stage s, a layer of $FeCl_3$ is regularly spaced between s layers of graphite (Dresselhaus & Dresselhaus, 1981; Solin, 1982; Ulloa & Kirczenow, 1986*a*, *b*). The $FeCl_3$ is particularly interesting because it appears to intercalate as a layer of the crystal (Cowley & Ibers, 1956; Metz & Schulze, 1975) which then remains incommensurate with its graphite host at room temperature. Furthermore, in stage $s \geq 2$, it is thought to be nearly uncorrelated from layer to layer as if one could slip a sandwich of $FeCl_3$, in which a central Fe layer is octahedrally coordinated with two layers of Cl (Wooster, 1932), in between two graphite hexagonal net planes with minimal host-intercalant interaction. In this study we have concentrated on the stage-4 $FeCl_3$-GIC where, in general for stage index s, we call the single group of s graphite planes separating the intercalant a 'set'. Fig. 1 shows a possible sequence of graphite sets and $FeCl_3$ for the stage-4 compound.

The formation of the stage structure is controlled by the temperature of the graphite host and the pressure of vaporized intercalant in contact with it. We can thus obtain the desired stage by controlling these conditions. The investigations of $FeCl_3$-GIC's have so far been carried out on samples quenched to room temperature from their high-temperature equilibrium state, at which temperature the intercalant may exist as a liquid or two-dimensional (2D) dense gas arrangement of molecules. Our current interest is in the X-ray determination of both the stacking sequence of the graphite layers and the structure of the $FeCl_3$ intercalant in stage-4 $FeCl_3$-GIC at elevated temperatures. In this paper, we confine our attention to the first issue and consider the intensity distribution along the c^* axis at various values of $\{H, K\}$; in a subsequent paper we will consider the in-plane intercalant structure.

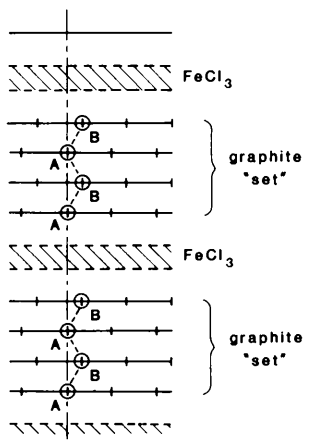

Fig. 1. Proposed stacking sequence of the graphite layers and the $FeCl_3$ intercalant in a stage-4 GIC. The stacking of graphite sets is shown as A-A; *i.e.* an A plane at the origin is followed after $FeCl_3$ by another A at the origin. (Across the $FeCl_3$ the *planes* are A/B.)

Studies of the stacking disorder in layered materials have been made by many investigators from both theoretical and experimental viewpoints; seminal among the former are the treatments of Hendricks & Teller (1942), Kakinoki & Komura (1965), Kakinoki (1967), Jagodzinski (1949) and Warren (1969). It would therefore be simplest for us to apply an appropriate version of one of these to our findings. However, the intensities we report here along the L lines in reciprocal space show a dependence on the $\{H, K\}$ Miller indices that has not been previously detailed, although Samuelsen, Moret, Fuzellier, Klatt, Lelaurain & Herold (1985) have reported similar effects in HNO_3-GIC's. We thus propose a new variation on the intensity analysis for these layered materials which gives a good fit to our data and provides some insight into staging.

II. Experimental

1. *Sample preparation*

A piece of highly oriented pyrolytic graphite (HOPG) of dimensions $8 \times 12 \times 0{\cdot}5$ mm was kindly supplied by Dr A. W. Moore with a c-axis mosaic spread of 0·5° FWHM (full width at half maximum). This was held in place in a thin-walled 12 mm diameter glass tube by two gently grooved 8 mm cylindrical glass tubes at the top and bottom, concentric with the outer tube and sealed to it. The bottom support tube was extended beyond the end of the thin-walled outer tube to make a cavity for $FeCl_3$. Three pieces of 99·9% pure iron wire were placed at the bottom of this composite tube. Because $FeCl_3$ is extremely hygroscopic, the tube was evacuated and repeatedly heated to ensure that no water remained. Chlorine gas was then introduced into the tube and the iron was heated slightly and reacted immediately to form $FeCl_3$. A residual chlorine atmosphere of 40 kPa was sealed inside the tube together with the graphite sample and the $FeCl_3$. The (composite) tube was held vertically in a two-zone furnace, mounted on the X-ray diffractometer, with the $FeCl_3$ heated to 495 K in the bottom part of the 8 mm tube while the graphite was held at 623 K. The intercalation to stage 4 took three days. The sample was centered at a window in the upper zone of the cylindrical furnace which allowed the X-ray beam to pass through and which was covered with a thin aluminium foil to prevent convection. The sample thickness was chosen so that, after intercalation, we would have a near optimal thickness for transmission measurements with Mo $K\alpha$ X-rays.

2. *X-ray measurements*

The X-ray generator was a Rigaku RU-200 with an Mo rotating anode in point focus geometry. The furnace was mounted on an x-y translation stage set on

a Huber diffractometer equipped with two (±20°) large goniometer arcs to allow for adjustment of the sample position. Two sodium iodide scintillation detectors were used, one of which monitored the incident beam which had been monochromated with vertically bent pyrolytic graphite. The (vertical) focus was at the sample position where the beam cross section was 2 mm (vertically) × 0·4 mm (horizontally, with a slit). The horizontal divergence of the incident beam due to the mosaic spread of the graphite monochromator was estimated to be less than 0·3° by measuring the profile of a silicon crystal reflection. The vertical divergence was 2°, which is not critically related to the resolution of the present intensity measurements which could all be made in a horizontal scattering plane. A 0·6 mm scatter slit was placed 3 cm from the sample which, together with a receiving slit of 0·3 mm, gave an angular acceptance of 0·1°. Vertically, the diffracted X-rays were restricted to 4°. (For the 10.L scan, the horizontal acceptance angle was 0·03°.)

As shown in Fig. 2, the Bragg peaks in a θ-2θ radial scan along a 00.L line have sharp profiles, including clear $K\alpha_1 - K\alpha_2$ splitting, indicating a good stage-4 periodicity along the c axis with no obvious trace of other stages. From this 00.L measurement, the lattice parameter c was determined to be 19·70(5) Å. By analyzing the 00.L integrated intensity data we also obtained the positional parameters of the graphite layers due to intercalation as well as the temperature factors. In the model calculation for the stacking disorder of the graphite layer sets, these refined parameters were adopted, but their influence was small and their discussion may be postponed. [The c-axis spacing may thus be treated as 3 × 3·35 Å plus a gallery spacing (d_s) of ~9·65 Å.] Fig. 3 shows a typical rocking curve of 00.L reflection which gives a measure of the mosaicity of the intercalated graphite sample at the elevated temperature. From this figure, the mosaic spread can be estimated to be ~1·8°. This mosaicity was small enough to permit an analysis of the profile distribution on $HK.L$ lines along the c^* axis, even though it had to be corrected for in analyzing the profiles, particularly for higher $\{H, K\}$ indices. θ-2θ radial scanning in the $HK.0$ plane gave the intensity distribution shown in Fig. 4. In this pattern, there are no peaks associated with the $FeCl_3$ crystal structure indicating that at 623 K the $FeCl_3$ molecules form a liquid whose detailed structure, which can be barely seen in the weak diffuse background, will be discussed in a later paper. (The glass sample tube scattering has been removed with slits.) The sharpness of the $HK.0$ graphite peaks (about 0·25° FWHM) shows that the internal structure of the graphite layers is comparable to that of the original HOPG.

$HK.L$ intensity distributions along the c^* axis were obtained in transmission on L lines at intervals of $\delta L = 0{\cdot}1$ from $L = -1{\cdot}5$ to $L = 10$. In analyzing the $HK.L$ intensity distribution, a monotonically varying background intensity (due mainly to liquid scattering from the $FeCl_3$ intercalant and Compton scattering) was treated as a linear function of L and subtracted

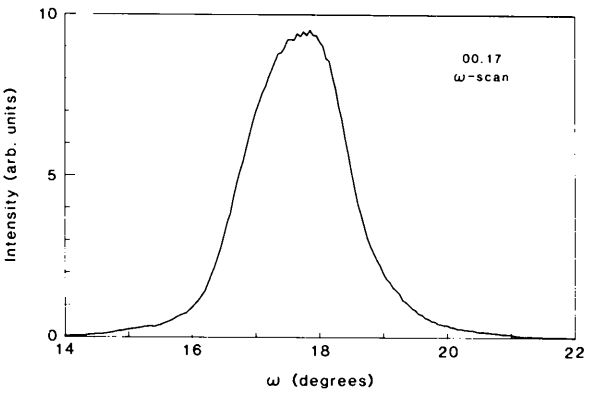

Fig. 3. Rocking curve at the 00.17 peak showing a mosaic spread whose FWHM ≈ 1·8°.

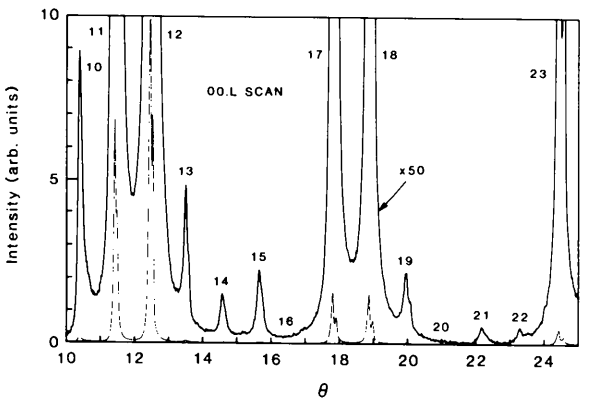

Fig. 2. Mo $K\alpha$ intensity distribution in a θ-2θ radial 00.L scan indicating a well staged sample for stage 4 with $c = 19{\cdot}70\,(5)$ Å. The $K\alpha_1 - K\alpha_2$ splitting is clear.

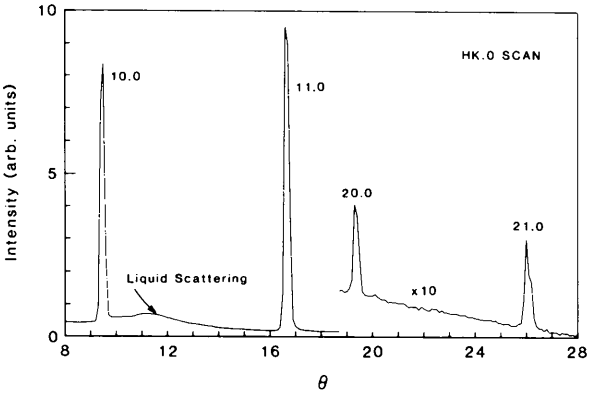

Fig. 4. θ-2θ radial scan in the $HK.0$ plane, indicating sharp in-plane graphite reflections and the absence of any $FeCl_3$ crystalline peaks. The weak diffuse bump peaking at $\theta \simeq 11{\cdot}3°$ is from the 2D $FeCl_3$ molecular liquid.

from the observed profiles so as to make the best fit to calculation. The observed intensity was then corrected for polarization and for an absorption factor for asymmetric transmission geometry. The instrumental peak broadening along L, associated both with the mosaicity of the sample (Kan, Misenheimer, Forster & Moss, 1987; Thompson, Moss & Misenheimer, 1988) and the resolution function due to the beam divergences in the optical system, was superposed on the calculated intensity distribution as part of the fitting procedure.

Fig. 5 shows the observed intensity profiles of the $HK.L$ reflections along lines of $\{H, K\} = \text{constant}$. Background intensities mentioned earlier have been subtracted from the data and polarization and absorption corrections have been made. Intensity scales are indicated in arbitrary units, but all intensities were normalized to the monitor counts of the incident X-ray beam and the relative intensities among the scans are correct. Included also in Fig. 5 are the fits to our model calculations, discussed in the following section.

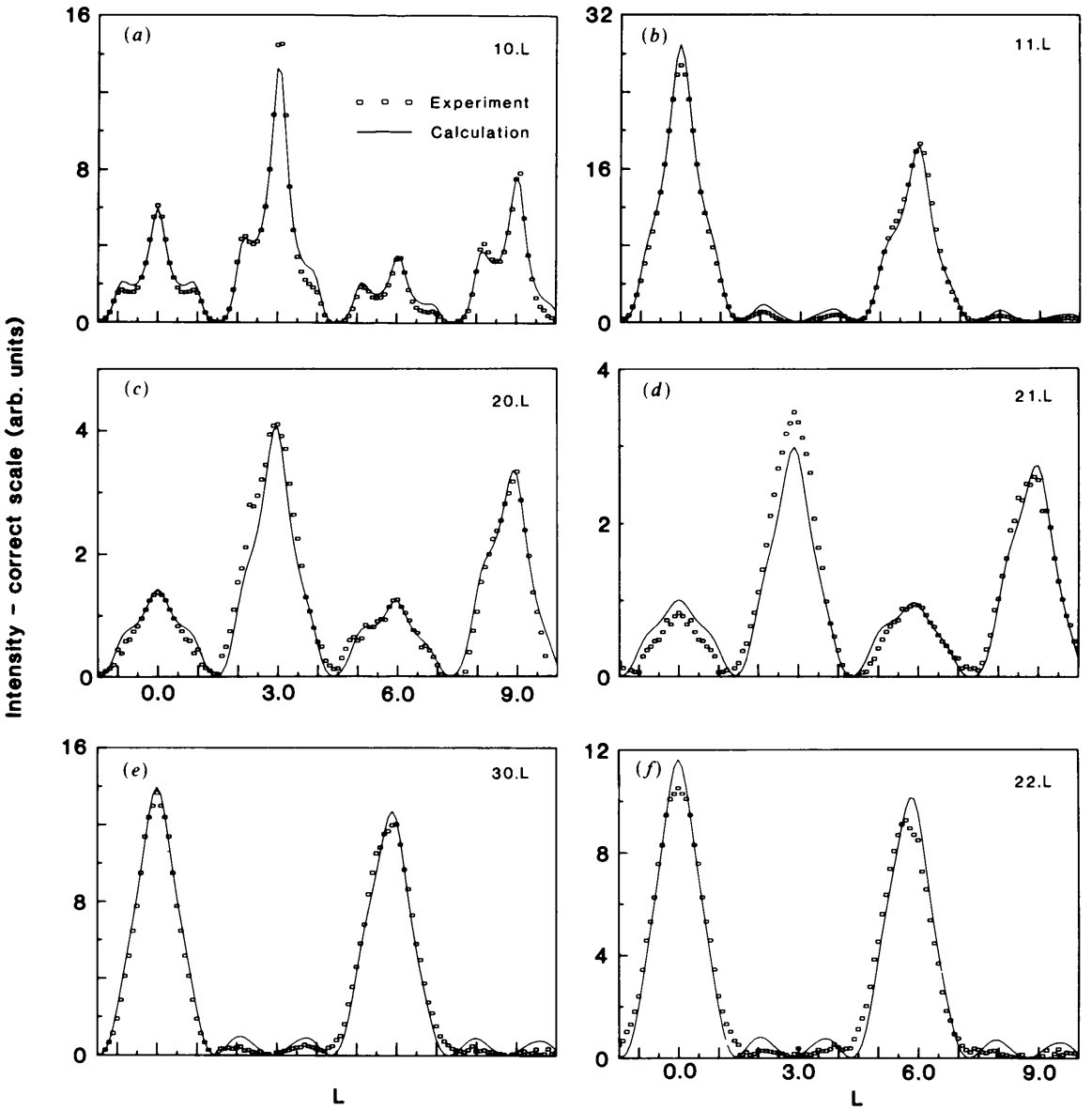

Fig. 5. Comparisons of observed and calculated intensity distributions for the (*a*) 10.*L*, (*b*) 11.*L*, (*c*) 20.*L*, (*d*) 21.*L*, (*e*) 30.*L* and (*f*) 22.*L* lines. The experimental points are all on one normalized intensity basis through monitor counting of I_0 and they are corrected for polarization and absorption effects. Background has also been subtracted. The model calculations are described in the text with model parameters given in Table 1.

It may easily be shown (Warren, 1969) that the $H-K=3n$ (n = integer) reflections have the same intensity distribution as the $00.L$ reflections under the condition that the shift vector between the graphite layer sets is one of the three A-, B- or C-type shift vectors in the xy plane $[0, \frac{1}{3}\mathbf{a}_1+\frac{2}{3}\mathbf{a}_2, \frac{2}{3}\mathbf{a}_1+\frac{1}{3}\mathbf{a}_2]$. Figs. 5($b$), ($e$) and ($f$), however, show broad profiles, in spite of sharp $00.L$ reflections, and thus require the existence of some random stacking of these sets. As distinguished from $H-K=3n$, the reflections of $H-K=3n\pm1$ may be broadened by stacking disorder as a result of a mixing of the A-, B- and/or C-type shift vectors. However, the random mixing of such regular vectors will not give any $\{H, K\}$ index dependence for those reflections. That is, $10.L$, $20.L$ and $21.L$ reflections necessarily have the same intensity distribution along L. Figs. 5(a), (c) and (d) display real differences in their L-dependent profiles and we therefore propose below a new model for stacking disorder in explanation of our data.

III. Structure model and calculation

The stage 4 structure is treated as an alternating sequence of sets of four (perfect) $ABAB$ graphite layers together with an $FeCl_3$ layer (see Fig. 1). We should notice, as mentioned in the last section, that the $11.L$, $22.L$ and $30.L$ reflections in Fig. 5 have considerably broader peaks than the $00.L$ intensity distribution in Fig. 2. This fact requires that the lateral correlation between the graphite layer sets along the c^* axis not extend to long inter-set distances. This short correlation length does not, however, mean that the three kinds of sequences of A-A, A-B and A-C between the sets are randomly mixed, because for such random mixings the $HK.L$ reflections of $H-K=3n$ retain sharp profiles. Thus, the broadening in the $H-K=3n$ profiles must be due to an interruption of A-A, A-B and/or A-C stacking of the graphite layer sets. This truncation of correlation over a short distance can be achieved in two distinct ways. One involves a rotational or twist disordering (Kan *et al.*, 1987) and the other involves a translational disorder as invoked by Samuelsen *et al.* (1985) for the ordered state of HNO_3 in graphite. For our data, translational disorder was incorporated in a model to explain the profiles; in staged materials with staggered domains (Ulloa & Kirczenow, 1986*a*, *b*) twist defects would not be energetically likely. Translational disorder caused by other than the definite A-A, A-B and A-C shift vectors should be formulated with some distribution function for the stacking probability, with fractional coordinates in the xy plane. This type of fractional stacking fault, which is required by the $H-K=3n$ reflections, will also help us understand the variation in the intensity distributions along the $H-K=3n\pm1$ lines; *i.e.* why the maxima along the $20.L$ line are broader than along $10.L$.

To reveal these features in the $HK.L$ intensity distributions, we construct the following model. If we put a set of $ABAB$ graphite layers at the origin (designated as 'A' because the A position is in the first plane), the first-neighbor layer set may in principle be placed randomly at any lateral (x, y) position in the next plane separated from the origin by the c lattice parameter. However, its in-plane positioning may not be completely random but rather may be limited to a definite distribution of correlation between the graphite layer sets, *i.e.* $W_1(X)$ [X standing for (x, y) in the plane normal to the c axis]. Here, we let $W_m(X)$, the probability function of finding an $ABAB$-type layer set at X in the mth neighbor plane when an $ABAB$ set is positioned at the origin plane, be represented by

$$W_m(X)=\int W_{m-1}(X')\,W_1(X-X')\,\mathrm{d}X'; \qquad (1)$$

that is, the case of '*Reichweite* $S=1$' is employed (Jagodzinski, 1949). We normalize $W_m(X)$ so that

$$\int W_m(X)\,\mathrm{d}X=1. \qquad (2)$$

The intensity scattered from this model structure can be written as

$$\begin{aligned} I(HK.L) &= \sum_s \sum_t V_s V_t^* \exp[-2\pi i L(s-t)] \\ &= \sum_s |V_s|^2 + 2\,\mathrm{Re}\sum\sum_{s<t} V_s V_t^* \\ &\quad \times \exp[-2\pi i L(s-t)], \end{aligned} \qquad (3)$$

where s and t are integer indices along the c axis. V_s

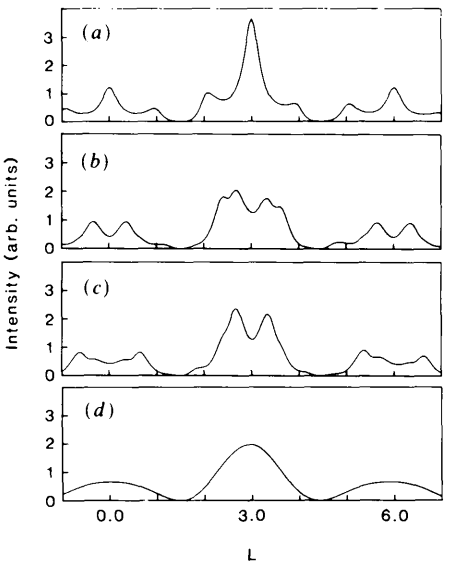

Fig. 6. Illustrative model intensity calculations for selected stacking sequences. The L dependence of the profile for an H, K reflection, $H-K=3n\pm1$ is shown for (a) $w_a=0{\cdot}3$, $w_d=0{\cdot}7$; (b) $w_b=0{\cdot}3$, $w_d=0{\cdot}7$; (c) $w_c=0{\cdot}3$, $w_d=0{\cdot}7$; (d) $w_d=1{\cdot}00$. In these calculations, the lateral distribution about each sequence is of zero width (see text).

is expressed as $V\exp(-2\pi i\varphi_s)$, where V is the structure factor for the graphite $ABAB$ layer set at the origin and $\varphi_s = Hx_s + Ky_s$ is due to the in-plane translation of the sth layer set. It should be noted that we have included no contribution of the $FeCl_3$ to the graphite Bragg peaks. While in principle such a contribution may exist (Reiter & Moss, 1986), were the $FeCl_3$ molecular liquid at 623 K more than weakly coupled to the graphite, the random lateral graphite shifts that we are modeling would probably not occur. In other words, a strong graphite-$FeCl_3$ interaction would tend to favor A-A, A-B or A-C stacking of sets. A weak coupling, such as obtains here, will produce negligible $FeCl_3$ contributions to the graphite peaks.

We further rewrite (3), assuming that the correlation length along c is much less than the crystal size, as

$$\begin{aligned} I(HK.L) &= N|V|^2 + 2N\,\mathrm{Re}\sum_{m>0}\langle V_s V^*_{s+m}\rangle\exp(2\pi iLm) \\ &= N|V|^2\left[1 + 2\,\mathrm{Re}\left\langle\sum_{m>0}\exp\{2\pi i(\varphi_{s+m}-\varphi_s)\}\right\rangle \right. \\ &\quad \left. \times\exp(2\pi iLm)\right] \\ &= N|V|^2\left[1 + 2\,\mathrm{Re}\sum_{m>0} W^*_m(H,K)\right. \\ &\quad \left.\times\exp(2\pi iLm)\right], \end{aligned} \tag{4}$$

$$W_m(H,K) = \int\int W_m(X)\exp[-2\pi i(Hx+Ky)]\,dx\,dy. \tag{5}$$

Here, the double summation in (3) is replaced by a single summation over m indicating the inter-set distance. $X \equiv (x, y)$ (x and y being continuous variables) and $\langle\ldots\rangle$ means the average over s with m fixed. N is the total number of graphite sets. Equation (5) can be developed according to (1) as

$$\begin{aligned} W_m(H,K) &= \int\int W_{m-1}(X')W_1(X-X') \\ &\quad\times\exp[-2\pi i(Hx+Ky)]\,dX'\,dX \\ &= W_{m-1}(H,K)W_1(H,K) \\ &= \{W_1(H,K)\}^m. \end{aligned} \tag{6}$$

This $W_m(H,K)$ is in general complex.

If we introduce a 60° rotation twinning about the c axis into the crystal, we have

$$I_{\mathrm{twin}}(HK.L) = \tfrac{1}{2}[I(HK.L) + I(KH.L)]. \tag{7}$$

This also corresponds to the intensity expression in the case of a rotational average of intensities with the same radial distance in reciprocal space, as realized in HOPG, except for a constant factor.

Before proceeding with the data analysis, we display in Fig. 6 the intensity modulations for the $H-K = 3n\pm1$ reflections arising from selected stacking sequences. Fig. 6(d) shows the perfectly disordered case in which every layer set can be located anywhere with the same probability in the next plane; (a) is for the case of an A-A stacking of sets in which the next layer set begins with exactly the A position with a probability of 30% with the rest distributed perfectly at random. Similarly, Fig. 6(b) shows an A-B stacking case with probability of 30% and (c) is for an A-C stacking case (30%).

The general features in the $H-K = 3n\pm1$ reflections observed with the present sample seem to be mainly characterized by the case in Fig. 6(a); this is a mixture of an A-A sequence of first-neighbor sets together with a random stacking of these sets [a mixture of staggered symmetric, as described by Ulloa & Kirczenow (1986a), and random]. The progressive broadening of the L-dependent peak profiles with increasing $\{H, K\}$ indices may be governed by a reduction of the contribution from the A-type stacking, *i.e.* by some distributed probability function around the A position in real space. Thus, we can compose a model structure sequence as the sum of a perfectly random component and a localized distribution around the A position. By extending this idea more generally to the B and C positions, we have a probability function $W_1(X)$ as

$$\begin{aligned} W_1(x) &= W_a(x,y) + W_b(x-\tfrac{1}{3}, y-\tfrac{2}{3}) \\ &\quad + W_c(x-\tfrac{2}{3}, y-\tfrac{1}{3}) + W_d, \end{aligned} \tag{8}$$

where $W_p(x', y')$ is a distribution function damping with increasing distance from the $x'=0$, $y'=0$ position. As a reasonable form for $W_p(x', y')$ we choose Cauchy functions and rewrite (8) as

$$\begin{aligned} W_1(X) &= (w_a\alpha/2)\exp[-\alpha d(x,y)] \\ &\quad + (w_b\beta/2)\exp[-\beta d(x-\tfrac{1}{3}, y-\tfrac{2}{3})] \\ &\quad + (w_c\gamma/2)\exp[-\gamma d(x-\tfrac{2}{3}, y-\tfrac{1}{3})] \\ &\quad + w_d, \end{aligned} \tag{9}$$

where a function $d(x', y')$ is defined as

$$d(x', y') = (x'^2 - x'y' + y'^2)^{1/2}, \tag{10}$$

representing the radial distance from the origin ($x' = 0$, $y' = 0$). Equation (9) satisfies (2) under the condition that $w_a + w_b + w_c + w_d = 1$, since (9) can be Fourier transformed into Lorentzian functions as

$$\begin{aligned} W_1(H,K) &= w_a/[1 + (2\pi/\alpha)^2 D^2(H,K)] \\ &\quad + w_b/[1 + (2\pi/\beta)^2 D^2(H,K)] \\ &\quad \times\exp[-2\pi i(H/3 + 2K/3)] \\ &\quad + w_c/[1 + (2\pi/\gamma)^2 D^2(H,K)] \\ &\quad \times\exp[-2\pi i(2H/3 + K/3)] \\ &\quad + w_d\delta(H,K), \end{aligned} \tag{11}$$

$$D(H, K) = [\tfrac{4}{3}(H^2 + HK + K^2)]^{1/2}. \quad (12)$$

w_a, w_b and w_c can be regarded as the total number density localized around each position in the xy plane. $D(H, K)$ is the radial distance in the HK plane in reciprocal space.

The model intensity distributions in Fig. 6 were calculated by setting the parameters as follows: (*a*) $w_a = 0{\cdot}3$, $w_b = w_c = 0$, $w_d = 0{\cdot}7$ and $\alpha = \infty$; (*b*) $w_b = 0{\cdot}3$, $w_a = w_c = 0$, $w_d = 0{\cdot}7$ and $\beta = \infty$; (*c*) $w_c = 0{\cdot}3$, $w_a = w_b = 0$, $w_d = 0{\cdot}7$ and $\gamma = \infty$; and (*d*) $w_a = w_b = w_c = 0$, $w_d = 1$. Equation (11) suggests that the index dependence of the intensity distribution for $H - K = 3n \pm 1$ can arise from the damping factors α, β, γ where the variation among them may change the weight of the contribution from each component. For the $H - K = 3n$ reflections, $\exp[-2\pi i(H/3 + 2K/3)]$ *etc.* in (11) are unity and there is no difference in intensity contribution among *A-A*, *A-B* and *A-C* stacking modes. That is, those intensity distributions can be determined only by the simple sum of the three contributions, which is equal to $(1 - w_d)$. For the $H - K = 3n \pm 1$ reflections, the first three terms are independent, since the coefficients $w_a/[1 + (2\pi/\alpha)^2 D^2(H, K)]$ *etc.* are positive. This suggests that an optimum set of coefficients can be determined as a mathematically unique solution. Thus, we can obtain the parameters w_a, w_b, w_c, α, β and γ by fitting the model intensity to the experimental profiles.

Were the data in Fig. 5 'perfect', this fitting could be effected by a least-squares procedure. In fact, we were best served by limiting the number of fitting parameters and finding the best - most physical - outcome by a trial-and-error procedure. Principal among our assumptions, which all of the fits essentially vindicated, was that $w_b = w_c = 0$. We then needed only to determine two parameters: the extent of the laterally distributed *A-A* sequence (α) and the relative weight of w_a ($w_d = 1 - w_a$). The final fitting parameters are in Table 1. Figs. 5(*a*)-(*f*) show the comparisons of our model calculations with the data.

In Fig. 5(*a*) the agreement is quite good overall. We are particularly pleased with the fit about $L = 0$ because it is there that the correction for the mosaic distribution (essentially parallel to the scan) must be made carefully. At $L = 3{\cdot}0$, $6{\cdot}0$ and $9{\cdot}0$, there are asymmetric shoulders at approximately $\delta L = \pm 1{\cdot}0$. These would all be symmetrical if the gallery spacing $d_s \equiv 3 \times 3{\cdot}35 = 10{\cdot}05$ Å. Here we have $d_s \simeq 9{\cdot}65$ Å. Were we to lower d_s to ~$9{\cdot}60$ Å, the agreement between model calculation and experiment would be nearly perfect (more asymmetric). In Figs. 5(*b*), (*e*) and (*f*) for $H - K = 3n$, the calculated intensity at $L = 2$ and 4 and $L = 8$ and 10 is larger than the experimental value. This seems real to us and is again due to a phasing of the kind noted above. Because the discrepancy is not crucial to our conclusions (or to the physics), we have left the fits as is. Perhaps the worst agreement is for the 21.*L* scan in Fig. 5(*d*) about $L = 0$ and $L = 3{\cdot}0$. While this intensity is weak and the mosaic effects are appreciable for higher (H, K), we really have no explanation for the discrepancy.

Table 1. *Optimum $W_1(H, K)$ values for each (H, K) reflection profile for the calculated curves in Fig. 5 and resultant parameters of the model*

FWHM(xy) refers to the Cauchy function $\exp[-\alpha d(x, y)]$ with its origin at the *A* position, given in units of the *a* lattice parameter.

(*a*) Optimum $W_1(H, K)$ values

H, K	$D(H, K)$	$W_1(H, K)$
1, 0	1·15	0·23
1, 1	2·00	0·10
2, 0	2·31	0·08
2, 1	3·06	0·05
3, 0	3·46	0·04
2, 2	4·00	0·03

(*b*) Resultant parameters

w_a	α	w_b	β	w_c	γ	w_d	FWHM (xy)
0·6	5·0	0	-	0	-	0·4	0·28

Overall, however, we are pleased with the agreement over the six *HK.L* profiles in Fig. 5. Table 1 shows that our sample contains 60% of a distributed *A-A* sequencing of nearest-neighbor sets across an $FeCl_3$ gallery - *i.e.* as in Fig. 1, but with a Cauchy distribution whose lateral width (FWHM) is $0{\cdot}28a$ or ~$0{\cdot}7$ Å. This *A-A* stacking is mixed with a 40% purely random sequencing of sets (complete sliding randomness of the graphite sets about $FeCl_3$). How this mixture is distributed in the physical crystal is not determined; but we would suspect that nearer the domain walls the randomness will spread. The broad Cauchy distribution is simply an attempt to characterize the rather weak *A-A* stacking tendency.

IV. Discussion

We assume with others (Ulloa & Kirczenow, 1986*a*, *b*) that the staging model of Daumas & Herold (1969) (D-H model) is an appropriate description of the arrangement of graphite and intercalant layers in the GIC's. This model allows for extended domains of intercalant species separated by domain walls in a (usually) staggered configuration that allows every graphite gallery, on average, to possess the same intercalant density. The width and energy of the domain walls is discussed in detail by Ulloa & Kirczenow (1986*a*) who explore the importance of the deformation of the graphite planes, proceeding from one domain to another, in stabilizing a particular domain structure. Our present results on stage-4 $FeCl_3$-GIC contribute to this discussion by providing evidence for a more disordered stacking of graphite sets in accommodating the intercalant.

It should be noted that our 11.*L* profile for stage 4 is considerably more diffuse than the corresponding

11.*L* profile reported by Metz & Schulze (1975) for $FeCl_3$ intercalated in a graphite single crystal to stage 3. This difference may be due to an intrinsic difference between the stacking perfection of HOPG and single-crystal graphite (Kan *et al.*, 1987) in which the basically disruptive intercalation proceeds in a more regular (ordered) way in the crystal. It may also be due to the fact that the single crystals are usually quite small (and thin) and can reach a stable stress-free equilibrium more readily than the bulkier HOPG. In either event, our HOPG intercalation produced a good single-stage compound, although we have not done a careful Hendricks & Teller (1942) analysis along 00.*L* to test for small amounts of (uniform) stage mixing. This well staged sample was held at 623 K for a period of a few weeks and did not 'heal' with time to produce sharper *HK.L* profiles along **c***. We must therefore assume that our sample represents at least a reasonably stable configuration of intercalant and graphite, and it can be regarded as a good stage 4 as far as the short correlation length of the present stacking sequence is concerned. (We have also intercalated another sample and found basically the same profiles as reported here.)

It is clear that relieving the requirement for exact crystalline stacking of the *ABAB* sets across the $FeCl_3$ layers provides a degree of freedom to the formation of D-H domains. There is a competition between a registered stacking of sets across the intercalant layer, induced both by host-intercalant interaction and by the symmetry of the graphite, and the elastic effects at domain walls which would favor the sliding of bounding layers. There seems to be no calculation of this competition although the treatment of Ulloa & Kirczenow (1986*a*, *b*) could be extended to cover it.

A physically appealing picture of such sliding disorder is given by Samuelsen *et al.* (1985). In Fig. 11 of their paper, they describe the shifting of the bounding planes about an ordered HNO_3 gallery in the stage-2 compound. The stacking proceeds $A/A'B'/B''A''/A'$ $(A''=A)$ whereby non-crystallographic shifts take A to A' *etc.* across the gallery. Samuelsen *et al.* (1985) postulate that the shifts follow a $+/-$ sequence to bring A back into registry with $A''=A$. In our case we make no such requirement. Stage 4 is defined solely by the number of graphite planes separating $FeCl_3$ without regard to their lateral position. The loss of lateral correlation is progressive, as described in § III.

The D-H model for $FeCl_3$ has received direct corroboration from the high-resolution electron-microscope observations of Thomas, Millward, Schlögl & Boehm (1980). These authors made cross-sectional electron micrographs to reveal directly the intercalant layers within the normal graphite lattice. They also showed some regions of domain or island formation with bending of the graphite planes about the intercalant islands.

Our results suggest that, either as a reasonably stable intermediate phase in the intercalation process, or as the final equilibrium D-H configuration, the stage-4 $FeCl_3$-GIC may be characterized at the temperature of intercalation by a substantial amount of translational randomness across the $FeCl_3$ layer. This translational randomness is mixed with ~60% of 'distributed' A-A ordering of the *ABAB* sets. Such a nearly complete randomness of the graphite bounding planes, while somewhat suprising, has also been observed in $CoCl_2$- and $NiCl_2$-GIC's (Wiesler, Suzuki & Zabel, 1988) where the ordered acceptor layers are translationally incommensurate but rotationally ordered with respect to the graphite host. We have also quenched the encapsulated stage-4 $FeCl_3$ compound to room temperature and examined both the intercalant structure and graphite stacking. Our initial results show clearly that, while the $FeCl_3$ has undergone incommensurate ordering within its gallery, the translational order of the graphite across the galleries has not substantially improved.

We thank Professor H. Zabel for helpful discussions. This research was supported by the National Science Foundation under Grant No. DMR-8603662.

References

COWLEY, J. M. & IBERS, J. A. (1956). *Acta Cryst.* **9**, 421-431.
DAUMAS, N. & HEROLD, A. (1969). *C. R. Acad. Sci. Ser. C*, **268**, 373-375.
DRESSELHAUS, M. S. & DRESSELHAUS, G. (1981). *Adv. Phys.* **30**, 139-326.
HENDRICKS, S. & TELLER, E. (1942). *J. Chem. Phys*, **10**, 147-167.
HOHLWEIN, D. & METZ, W. (1974). *Z. Kristallogr.* **139**, 279-296.
JAGODZINSKI, H. (1949). *Acta Cryst.* **2**, 201-207, 208-214, 298-304.
KAKINOKI, J. (1967). *Acta Cryst.* **23**, 875-888.
KAKINOKI, J. & KOMURA, Y. (1965). *Acta Cryst.* **19**, 137-147.
KAN, X. B., MISENHEIMER, M. E., FORSTER, K. & MOSS, S. C. (1987). *Acta Cryst.* A**43**, 418-425.
METZ, W. & HOHLWEIN, D. (1975). *Carbon*, **13**, 87-96.
METZ, W. & SCHULZE, E. J. (1975). *Z. Kristallogr.* **142**, 409-422.
MORET, R. (1986). In *Intercalation in Layered Materials*, edited by M. S. DRESSELHAUS. *NATO ASI Series B, Physics*, Vol. 148, pp. 185-211.
REITER, G. & MOSS, S. C. (1986). *Phys. Rev. B*, **33**, 7209-7217.
SAMUELSEN, E. J., MORET, R., FUZELLIER, H., KLATT, M., LELAURAIN, M. & HEROLD, A. (1985). *Phys. Rev. B*, **32**, 417-427.
SOLIN, A. (1982). *Adv. Chem. Phys.* **49**, 455-532.
THOMAS, J. M., MILLWARD, G. R., SCHLÖGL, R. F. & BOEHM, H. P. (1980). *Mater. Res. Bull.* **15**, 671-676.
THOMPSON, C., MOSS, S. C. & MISENHEIMER, M. E. (1988). *Phys. Rev. B.* In the press.
ULLOA, S. E. & KIRCZENOW, G. (1986*a*). *Phys. Rev. B*, **33**, 1360-1371.
ULLOA, S. E. & KIRCZENOW, G. (1986*b*). *Comm. Condensed Matter Phys.* **12**, 181-189.
WARREN, B. E. (1969). *X-ray Diffraction.* Reading, MA: Addison-Wesley.
WIESLER, D. G., SUZUKI, M. & ZABEL, H. (1988). *Phys. Rev. B.* In the press.
WOOSTER, N. (1932). *Z. Kristallogr.* **83**, 35-41.